RESEARCH PAPER

Targeted Nose-to-Brain Delivery Using Functionalized Nanoparticles for Cognitive Restoration in Alzheimer's Disease

Virupaxappa Biradar[1], Giridhar Kunamaneni[2], Nina Varghese[3], B. Hema Kiranmayi[4], Boboxonova Muhayyoxon Mo'minjonovna[5], Madjidova Gulbaxor Tolibovna[6], Jeevanandham Somasundaram[7*]

[1]Department of General Medicine, Shri BM Patil Medical College Hospital & Research Centre, Vijayapura.
[2]Northeastern University, 360 Huntington Ave, Boston, Massachusetts 02115, USA.
[3]Faculty of Pharmacy, AIMST University, 08100 Bedong, Kedah, Malaysia.
[4]Aditya College of Pharmacy, Surampalem – 533437, Andhra Pradesh, India.
[5]Department of Folk Medicine and Pharmacology, Fergana Medical Institute of Public Health, Yangi Turon, Fergana – 150100, Uzbekistan.
[6]Department of Internal Diseases and Cardiology No2, Samarkand State Medical University, Samarkand, Uzbekistan.
[7]Sri Shanmugha College of Pharmacy (affiliated with The Tamil Nadu Dr. M.G.R. Medical University, Chennai), Pullipalayam, Morur (Po), Sankari (Tk), Salem District, Tamil Nadu – 637 304, India.

***Corresponding Author:**
Dr. Jeevanandham Somasundaram,
Director, Professor of Pharmaceutics,
Sri Shanmugha College of Pharmacy, (affiliated with The Tamil Nadu Dr.M.G.R. Medical University, Chennai),
Pullipalayam, Morur(Po),
Sankari (Tk), Salem district, Tamil Nadu - 637 304, India.
spjeeva1983@gmail.com

Abstract

Alzheimer's disease (AD) represents the most prevalent and devastating form of age-related neurodegenerative disorder, characterized by progressive cognitive decline, memory impairment, and neuropsychiatric symptoms that arise from the accumulation of amyloid-beta (Aβ) plaques, neurofibrillary tau tangles, and chronic neuroinflammation. A major obstacle in the pharmacological management of AD is the inability of most therapeutic agents to cross the blood-brain barrier (BBB) in therapeutically meaningful concentrations following conventional systemic administration. The present investigation focuses on the design, fabrication, and comprehensive in vitro characterization of functionalized polymeric nanoparticles (NPs) loaded with Donepezil hydrochloride (DPZ), a first-line acetylcholinesterase inhibitor, intended for intranasal delivery as a novel cognitive restoration platform in Alzheimer's disease. Poly(lactic-co-glycolic acid) (PLGA) and chitosan were selected as the primary polymeric matrices and surface-functionalization agents, respectively, owing to their well-established biocompatibility, biodegradability, mucoadhesive properties, and ability to enhance cellular uptake. Eight distinct nanoparticle formulations (F1–F8) were systematically developed by varying PLGA concentration, chitosan coating levels, drug-to-polymer ratios, and the addition of stabilizers such as polyvinyl alcohol (PVA). The formulations were evaluated for particle size, polydispersity index (PDI), zeta potential, encapsulation efficiency (EE%), drug loading (DL%), in vitro drug release behavior using Franz diffusion cells, mucoadhesive strength, and ex vivo nasal permeation. Optimized formulations demonstrated particle sizes in the range of 145–310 nm, positive zeta potentials (due to chitosan coating), encapsulation efficiencies exceeding 72%, and sustained biphasic drug release profiles extending over 24 hours, with enhanced mucoadhesive properties suitable for prolonged olfactory epithelium contact time. The results demonstrate that chitosan-coated PLGA nanoparticles represent an effective and tunable platform for nose-to-brain delivery of anti-Alzheimer drugs, with significant potential for advancing translational research in neurodegenerative disease therapy.

Keywords: Alzheimer's disease; nose-to-brain delivery; PLGA nanoparticles; chitosan; intranasal drug delivery; blood-brain barrier; donepezil.

How to cite this article: Biradar V, Kunamaneni G, Varghese N, Hema Kiranmayi B, Mo'minjonovna BM, Tolibovna MG, Somasundaram J. Targeted Nose-to-Brain Delivery Using Functionalized Nanoparticles for Cognitive Restoration in Alzheimer's Disease. Int J Drug Deliv Technol. 2026;16(21s): 964-977. DOI: 10.25258/ijddt.16.21s.101

1. Introduction

Alzheimer's disease (AD) is a chronic, progressive, and irreversible neurodegenerative disorder that represents the leading cause of dementia worldwide, accounting for approximately 60–70% of all dementia cases. The global burden of AD is staggering: as of 2023, more than 55 million individuals live with dementia globally, with projections estimating this number will exceed 139 million by 2050, driven primarily by rapid population aging. Beyond the enormous human suffering and caregiver burden it imposes, AD exerts an immense socioeconomic impact, with annual costs of care estimated to surpass USD 1.3 trillion globally. Despite decades of intensive research, no disease-modifying treatment capable of halting or reversing the neurodegenerative cascade has yet been successfully translated to clinical practice, underscoring the critical urgency for novel and efficacious therapeutic approaches.[1,2]

The neuropathological hallmarks of AD are well-characterized and include the extracellular deposition of amyloid-beta (Aβ) plaques derived from aberrant processing of the amyloid precursor protein (APP), intraneuronal accumulation of hyperphosphorylated tau protein forming neurofibrillary tangles (NFTs), widespread synaptic dysfunction, cholinergic neuronal degeneration in the basal forebrain, and progressive cortical and hippocampal atrophy. The cholinergic hypothesis, one of the earliest mechanistic frameworks established for AD, posits that the selective loss of cholinergic neurons in the nucleus basalis of Meynert and consequent reduction in acetylcholine (ACh) neurotransmission underlie the cognitive deficits observed in patients. This hypothesis provided the pharmacological rationale for the development of acetylcholinesterase inhibitors (AChEIs), such as donepezil, rivastigmine, and galantamine, which remain the mainstay of symptomatic pharmacotherapy in mild-to-moderate AD.[3,4]

The most formidable pharmacological challenge in AD therapeutics is the presence of the blood-brain barrier (BBB), a highly selective neurovascular structure composed of tightly joined brain microvascular endothelial cells, astrocytic end-feet, pericytes, and the associated basement membrane. The BBB strictly regulates the passage of molecules between the systemic circulation and the central nervous system (CNS) parenchyma, permitting only small, lipophilic, non-ionized molecules with molecular weights below approximately 400–500 Da to diffuse passively. The vast majority of potentially neuroprotective and disease-modifying agents—including peptides, antibodies, antisense oligonucleotides, gene therapy constructs, and many small-molecule drugs—fail to achieve adequate CNS bioavailability following conventional oral or intravenous administration due to BBB impermeability, rapid systemic metabolism, and first-pass hepatic clearance. Furthermore, the high doses required to achieve CNS-effective plasma concentrations via systemic routes often lead to unacceptable peripheral adverse effects, limiting dose escalation and long-term treatment adherence.[5,6]

Intranasal (IN) drug delivery has gained substantial scientific and clinical momentum as an elegant non-invasive strategy to circumvent the BBB and enable direct nose-to-brain drug transport. The nasal cavity provides unique anatomical access to the brain via two primary neural conduits: the olfactory nerve pathway and the trigeminal nerve pathway. The olfactory epithelium, located in the superior turbinate region of the nasal cavity, contains specialized bipolar sensory neurons whose unmyelinated axons project through the cribriform plate of the ethmoid bone directly to the olfactory bulb, which connects to limbic brain regions including the entorhinal cortex, hippocampus, and amygdala—areas critically affected in AD. The trigeminal nerve, with branches innervating the nasal mucosa, provides an additional neural highway connecting nasal epithelium with brainstem and higher cortical regions. Drug molecules deposited in the olfactory region can be transported along these pathways via both intraneuronal (axonal) and perineural (extracellular) mechanisms, bypassing systemic circulation entirely.[7,8]

Despite the compelling anatomical rationale for intranasal brain targeting, the nasal route presents significant biophysical challenges. The nasal mucosa is continuously bathed in mucus secreted by goblet cells, containing mucin glycoproteins, enzymes, and immunoglobulins that can trap drug molecules and restrict their access to the epithelial surface. Mucociliary clearance, driven by ciliated epithelial cells beating at approximately 1000 cycles per minute, sweeps deposited substances toward the nasopharynx at a rate of approximately 5–6 mm/min, dramatically limiting drug residence time. Nasal enzymatic degradation by peptidases, proteases, and cytochrome P450 enzymes further compromises the stability of peptide and protein therapeutics. The olfactory epithelium constitutes only a small fraction—approximately 5–10 cm^2—of the total nasal mucosal surface area (approximately 150–160 cm^2 in humans), and achieving consistent drug deposition in this region with conventional nasal formulations (drops, sprays) is technically challenging.[9,10]

Nanotechnology-based drug delivery systems, particularly polymeric nanoparticles (NPs), offer a transformative platform to overcome these intranasal delivery barriers while simultaneously enhancing nose-to-brain targeting efficiency. Nanoparticles in the size range of 50–500 nm can

interact productively with the nasal mucosa, exploit transcellular and paracellular transport pathways, resist mucociliary clearance due to mucoadhesive surface properties, protect encapsulated drugs from enzymatic degradation, and enable controlled and sustained drug release at the target site. Surface functionalization of nanoparticles with mucoadhesive polymers such as chitosan, thiolated chitosan, hyaluronic acid, or cell-penetrating peptides dramatically augments their nasal mucosal retention, facilitates endocytic uptake by olfactory neurons, and enhances transcytosis across olfactory sustentacular cells.[11,12]

Poly(lactic-co-glycolic acid) (PLGA) is the most extensively investigated biodegradable polymer in pharmaceutical nanotechnology and has received regulatory approval from the U.S. FDA for use in injectable formulations. PLGA undergoes hydrolytic degradation in biological environments via ester bond cleavage, producing lactic acid and glycolic acid—both endogenous metabolites—ensuring excellent biocompatibility and safety. The degradation rate, and consequently drug release kinetics, can be precisely tuned by altering the lactic acid:glycolic acid (LA:GA) ratio, molecular weight, and end-group chemistry. Donepezil hydrochloride, a second-generation AChEI with high oral bioavailability (approximately 100%) but only moderate CNS penetration (CSF:plasma ratio ~0.56), represents an ideal candidate for nose-to-brain nanoparticulate delivery, as encapsulation in PLGA nanoparticles could enhance its olfactory epithelium permeation and provide sustained hippocampal drug levels with reduced peripheral cholinergic side effects.[13,14]

The present study was conceived to address these critical gaps by developing and characterizing a panel of eight chitosan-functionalized PLGA nanoparticle formulations (F1–F8) loaded with Donepezil hydrochloride, systematically exploring the effects of polymer concentration, chitosan coating, drug loading, and PVA stabilizer levels on physicochemical properties, encapsulation efficiency, in vitro drug release, mucoadhesive strength, and ex vivo nasal permeation. The overarching goal is to identify an optimized nanoparticulate formulation strategy with maximum potential for translation toward a nose-to-brain delivery system capable of restoring cognitive function in Alzheimer's disease patients.[15]

2. Materials

Donepezil hydrochloride (DPZ; purity ≥99.5%, MW 415.96 g/mol) was procured as a gift sample from Sun Pharmaceutical Industries Ltd. (Mumbai, India). Poly(lactic-co-glycolic acid) (PLGA; LA:GA ratio 50:50, Mw 30,000–60,000 Da, Resomer® RG 503H) was obtained from Sigma-Aldrich Co. LLC (St. Louis, MO, USA). Low molecular weight chitosan (LMW; degree of deacetylation ≥85%, viscosity 20–300 mPa·s, Sigma-Aldrich, USA) and medium molecular weight chitosan (MMW; degree of deacetylation ≥75%, Sigma-Aldrich, USA) were used for nanoparticle surface coating and ionic gelation. Polyvinyl alcohol (PVA; MW 31,000–50,000 Da, 87–89% hydrolyzed) was purchased from Sigma-Aldrich (USA) and served as a steric stabilizer in the aqueous phase. Poloxamer 188 (Pluronic® F68) was sourced from BASF SE (Ludwigshafen, Germany). Acetonitrile (HPLC grade, ≥99.9%) and methanol (HPLC grade, ≥99.9%) were obtained from Merck KGaA (Darmstadt, Germany). Dichloromethane (DCM; analytical grade, ≥99.8%) and acetone (analytical grade, ≥99.5%) were purchased from Loba Chemie Pvt. Ltd. (Mumbai, India) and used as organic solvents for nanoparticle preparation. Dialysis membranes (Spectra/Por®, MWCO 12,000–14,000 Da) were obtained from Spectrum Laboratories Inc. (Rancho Dominguez, CA, USA) and used for in vitro drug release studies. Phosphate-buffered saline (PBS, pH 6.4, 7.4) was prepared in-house using sodium chloride, potassium chloride, disodium hydrogen phosphate, and potassium dihydrogen phosphate procured from Himedia Laboratories Pvt. Ltd. (Mumbai, India). Mucin (Type II, partially purified, from porcine stomach) was obtained from Sigma-Aldrich (USA) and used for mucoadhesion assessment. Tripolyphosphate sodium (TPP; ≥97.0%) was sourced from Sigma-Aldrich (USA) and employed as an ionic cross-linking agent for chitosan. Bovine serum albumin (BSA) was procured from HiMedia (Mumbai, India). All other reagents and chemicals used throughout the study were of analytical or HPLC grade unless otherwise specified. Purified water (resistivity ≥18.2 MΩ·cm) was produced using a Milli-Q water purification system (Millipore, Bedford, MA, USA) and used for all aqueous preparations.

3. Methods

3.1 Preparation of Drug-Loaded PLGA Nanoparticles by Nanoprecipitation

PLGA nanoparticles encapsulating Donepezil hydrochloride (DPZ) were fabricated using the solvent nanoprecipitation technique, which produces nanoparticles with high uniformity and reproducibility without the need for high-energy mechanical processing. Briefly, accurately weighed quantities of PLGA (50–100 mg, varying by formulation) and DPZ (10–30 mg) were co-dissolved in 10 mL of acetone/dichloromethane (1:1, v/v) mixture under continuous magnetic stirring at 600 rpm and room temperature until a clear, homogeneous organic solution was obtained. This organic phase was then injected

dropwise at a controlled rate of 1 mL/min using a syringe pump into 25 mL of an aqueous phase containing PVA (0.5–2% w/v, varying by formulation) and Poloxamer 188 (0.1% w/v) under constant mechanical stirring at 800 rpm using a high-speed overhead stirrer. The instantaneous solvent diffusion upon contact between the organic and aqueous phases precipitated the polymer, entrapping the drug within the nascent nanoparticulate matrix. The organic solvents were subsequently removed by evaporation under reduced pressure using a rotary evaporator (Büchi R-300, Switzerland) at 30°C for 3–4 hours until a stable milky colloidal dispersion was obtained. The resulting nanoparticle suspension was then subjected to further processing for surface coating or direct characterization as specified.[16,17]

3.2 Emulsification-Solvent Evaporation Method for Selected Formulations

For formulations requiring encapsulation of the hydrochloride salt form of DPZ with enhanced efficiency, a modified double-emulsion (water-in-oil-in-water; W/O/W) solvent evaporation method was employed. An aqueous solution of DPZ (100–200 µL, 5% w/v in purified water) was emulsified with 2 mL of PLGA solution in DCM (5–10% w/v) using a probe sonicator (Sonics Vibra-Cell, USA) at 40% amplitude for 60 seconds in an ice bath to form the primary W_1/O emulsion. This primary emulsion was immediately poured into 20 mL of aqueous PVA solution (1–2% w/v) under vortexing, followed by probe sonication at 40% amplitude for 120 seconds to form the secondary $W_1/O/W_2$ double emulsion. The double emulsion was transferred to a magnetic stirrer and stirred continuously overnight (12–16 hours) at room temperature under a partial vacuum to allow complete evaporation of DCM. The hardened nanoparticles were collected by ultracentrifugation at 18,000 rpm for 30 minutes at 4°C (Beckman Coulter Optima LE-80K, USA), washed twice with purified water to remove residual PVA and unentrapped drug, and resuspended in 5 mL of purified water for further characterization.[18]

3.3 Chitosan Surface Coating via Ionic Interaction

To impart positive surface charge, enhance mucoadhesion, and improve cellular uptake, selected formulations were surface-coated with chitosan using an ionic interaction-based post-coating strategy. A stock solution of low molecular weight chitosan (0.1–0.5% w/v) was prepared in aqueous acetic acid (1% v/v) and pH-adjusted to 5.0–5.5 using sodium hydroxide (0.1 M). The freshly prepared, washed PLGA nanoparticle suspension was added dropwise to the chitosan solution under gentle magnetic stirring (300–400 rpm) to achieve a nanoparticle:chitosan weight ratio of 1:0.1 to 1:0.5 (varying by formulation). The mixture was incubated for 1 hour at room temperature with continuous stirring to allow electrostatic adsorption of positively charged chitosan chains onto the negatively charged PLGA nanoparticle surface. The chitosan-coated nanoparticles were then recovered by centrifugation at 15,000 rpm for 20 minutes, washed with water, and resuspended. The coating was further stabilized in certain formulations using sodium tripolyphosphate (TPP; 0.5 mg/mL) as an ionic cross-linker added at a final concentration of 1:5 (chitosan:TPP molar ratio), promoting physical cross-linking of the chitosan shell.[19,20]

3.4 Particle Size, PDI, and Zeta Potential Measurement

The hydrodynamic diameter (Z-average particle size), polydispersity index (PDI), and zeta potential (ζ) of all nanoparticle formulations were determined using dynamic light scattering (DLS) and electrophoretic light scattering (ELS) techniques, respectively, employing a Malvern Zetasizer Nano ZS instrument (Malvern Panalytical, Worcestershire, UK) equipped with a 4 mW He-Ne laser (λ = 633 nm) and a non-invasive backscatter (NIBS) detection geometry at 173°. Prior to measurement, nanoparticle suspensions were diluted 1:100 in purified water or PBS (pH 6.4) to achieve an appropriate scattering intensity (typically 200–400 kcps). Each measurement was performed in triplicate at 25°C with a 120-second equilibration time. Particle size and PDI were derived from intensity-weighted autocorrelation function analysis using the cumulant algorithm. Zeta potential was calculated from the measured electrophoretic mobility using the Henry equation with the Smoluchowski approximation ($f(\kappa a) = 1.5$) appropriate for nanoparticles in aqueous media of moderate ionic strength.[21]

3.5 Transmission Electron Microscopy (TEM) for Morphological Analysis

The morphology, surface texture, and core-shell architecture of representative nanoparticle formulations (F4 and F7 as uncoated and chitosan-coated counterparts) were examined by transmission electron microscopy (TEM; JEOL JEM-2100F, Japan) operating at an accelerating voltage of 200 kV. Nanoparticle suspensions were diluted 10-fold in purified water, and a 10 µL aliquot was deposited onto a carbon-coated copper TEM grid (300 mesh, Ted Pella Inc., USA). Excess liquid was blotted after 1 minute, and the grid was negatively stained with 2% (w/v) aqueous phosphotungstic acid solution (pH 7.0) for 60 seconds. The stained grids were air-dried at room temperature for 24 hours before TEM analysis. Images were acquired at magnifications ranging from 50,000× to 200,000×, and particle size distributions were measured from TEM

micrographs using ImageJ software (NIH, USA) by analyzing at least 100 individual particles per formulation.[22]

3.6 Encapsulation Efficiency and Drug Loading Determination

Encapsulation efficiency (EE%) and drug loading (DL%) of each nanoparticle formulation were determined by an indirect method using high-performance liquid chromatography (HPLC). Following ultracentrifugation of the nanoparticle suspension at 18,000 rpm for 30 minutes (Beckman Coulter), the supernatant containing free (unentrapped) drug was carefully separated. The drug concentration in the supernatant (C_free) was quantified by HPLC after appropriate dilution. Encapsulation efficiency was calculated using the formula: EE% = [(C_total – C_free) / C_total] × 100, where C_total is the theoretical total drug concentration in the formulation. Drug loading was calculated as: DL% = [(Mass of drug in NPs) / (Total mass of NPs)] × 100. The nanoparticle pellet was dissolved in acetonitrile (1 mL) under ultrasonication, diluted with mobile phase, and total drug content confirmed by HPLC. The validated HPLC method employed a C_{18} reverse-phase column (Phenomenex Luna C18, 250 × 4.6 mm, 5 µm particle size) with a mobile phase consisting of acetonitrile:0.1% trifluoroacetic acid in water (60:40, v/v) at a flow rate of 1.0 mL/min, column temperature of 30°C, and UV detection at 268 nm. The method was validated for linearity, accuracy, precision, and specificity over a concentration range of 1–100 µg/mL ($R^2 > 0.9998$).[23,24]

3.7 FTIR Spectroscopic Analysis for Drug-Polymer Interaction Study

Fourier-transform infrared (FTIR) spectroscopy was employed to investigate potential physicochemical interactions between DPZ, PLGA, and chitosan, and to confirm successful drug encapsulation and polymer coating. FTIR spectra were recorded for pure DPZ, PLGA, chitosan (LMW), physical mixture of DPZ+PLGA, physical mixture of DPZ+PLGA+chitosan, uncoated DPZ-PLGA nanoparticles (F4), and chitosan-coated DPZ-PLGA nanoparticles (F7). Lyophilized nanoparticle powders and drug/polymer samples were prepared as KBr pellets (1 mg sample in 100 mg KBr), and spectra were recorded using a Shimadzu IRAffinity-1 FTIR spectrophotometer (Japan) over the wavenumber range of 4000–400 cm^{-1} at a resolution of 4 cm^{-1}, with 32 accumulative scans per spectrum. Key characteristic absorption bands for DPZ (N-H stretch, C=O ester, aromatic C=C, piperidine N-CH_2), PLGA (carbonyl ester C=O at ~1756 cm^{-1}, C-O-C stretch), and chitosan (O-H/N-H broad band at 3200–3600 cm^{-1}, amide I C=O at ~1650 cm^{-1}, amide II N-H at ~1550 cm^{-1}) were identified and compared across all spectra to detect shifts, broadening, or disappearance of bands indicative of molecular interactions.[25]

3.8 Differential Scanning Calorimetry (DSC) for Thermal Analysis

Differential scanning calorimetry (DSC) was performed to assess the physical state of DPZ within the nanoparticle matrix and to investigate any thermal transitions indicating drug-polymer interactions or alteration of drug crystallinity upon encapsulation. DSC thermograms were obtained for pure DPZ, PLGA, chitosan, physical mixture (DPZ + PLGA + chitosan, 1:5:0.5 w/w), lyophilized uncoated PLGA-NPs (F4), and lyophilized chitosan-coated PLGA-NPs (F7) using a DSC 8500 instrument (PerkinElmer Inc., Waltham, MA, USA). Samples (3–5 mg) were weighed accurately into sealed aluminum pans and heated from 30°C to 300°C at a heating rate of 10°C/min under a continuous nitrogen purge (50 mL/min) to prevent oxidative degradation. The instrument was calibrated with indium (melting point 156.6°C, ΔHf = 28.6 J/g) and zinc (melting point 419.5°C) standards. The characteristic melting endotherm of DPZ (reported at ~228–230°C) was examined in all samples to assess drug crystallinity status and evaluate whether amorphization or solid dispersion formation occurred during nanoparticle preparation.[26]

3.9 X-Ray Powder Diffractometry (XRPD)

X-ray powder diffraction analysis was carried out to complement DSC findings and further characterize the crystalline or amorphous state of DPZ within the nanoparticle matrix. XRPD patterns were recorded for pure DPZ, PLGA, physical mixture, lyophilized F4, and lyophilized F7 using a PANalytical X'Pert PRO diffractometer (Netherlands) with CuKα radiation (λ = 1.5406 Å) generated at 40 kV and 40 mA. Diffraction patterns were collected over a 2θ range of 5°–50° at a scan speed of 2°/min with a step size of 0.02°. The pure drug characteristically exhibited sharp, well-defined diffraction peaks at 2θ values of approximately 11.8°, 14.2°, 18.6°, 22.3°, 24.7°, and 27.1°, reflecting its semicrystalline nature. Disappearance or significant broadening of these peaks in nanoparticle formulations was taken as evidence of drug amorphization or conversion to a molecularly dispersed state within the polymer matrix—both desirable for enhancing dissolution rate and absorption across the nasal mucosa.[27]

3.10 In Vitro Drug Release Studies Using Dialysis Membrane

The in vitro cumulative drug release profiles from all eight nanoparticle formulations were evaluated using a dialysis membrane diffusion technique. A precisely measured volume of nanoparticle suspension equivalent to 5 mg of

DPZ was sealed within pre-swollen dialysis bags (MWCO 12,000–14,000 Da) and placed in 500 mL of PBS (pH 6.4, simulating nasal fluid) contained in a USP Type-II dissolution apparatus (Electrolab EDT-08Lx, India) at 37 ± 0.5°C with a paddle rotation speed of 50 rpm. PBS (pH 6.4) was selected to mimic the physiological pH of the nasal cavity. Aliquots of 5 mL were withdrawn at predetermined time intervals (0.25, 0.5, 1, 2, 4, 6, 8, 12, 24 hours) and replaced with equal volumes of fresh PBS to maintain sink conditions. Withdrawn samples were filtered through 0.22 µm PVDF syringe filters, diluted appropriately, and analyzed by the validated HPLC method described in Method 3.6. The cumulative percentage drug released at each time point was calculated and plotted as a function of time. Drug release kinetics were modeled by fitting release data to zero-order, first-order, Higuchi matrix, Korsmeyer-Peppas, and Hixson-Crowell models using DDSolver software add-in (Microsoft Excel) to determine the prevailing release mechanism.[28,29]

3.11 Mucoadhesion Study Using Texture Profile Analysis

The mucoadhesive strength of the nanoparticle formulations was quantitatively assessed using texture profile analysis (TPA) employing a TA.XT Plus Texture Analyser (Stable Micro Systems, Surrey, UK) equipped with a 5 kg load cell and a stainless-steel cylindrical probe (10 mm diameter). A 2% w/v aqueous mucin (Type II, porcine stomach, Sigma-Aldrich) solution in PBS (pH 6.4) was used as a mucin disc substrate to simulate nasal mucosal surface. Mucin solution (2 g) was evenly spread on a flat glass disc (diameter 50 mm), allowed to gel slightly at 4°C for 1 hour, and fixed onto the TA base plate. A 200 µL volume of nanoparticle suspension was evenly applied to the probe surface. The probe was lowered onto the mucin gel at a speed of 0.5 mm/s, maintained in contact with a contact force of 0.05 N for 120 seconds to allow adhesive bond formation, and then retracted at 0.5 mm/s. The force-time curve generated was analyzed for maximum detachment force (peak adhesive force, mN) and work of adhesion (area under the curve, mJ). Each formulation was tested in triplicate (n = 3), and plain nanoparticles without chitosan coating (F1, F2) served as controls. An adhesion index (AI) was calculated as the ratio of mucoadhesive work of the test formulation relative to plain PLGA-NP (F1).[30]

3.12 *Ex Vivo* Nasal Permeation Study

Ex vivo permeation of DPZ across freshly excised sheep nasal mucosa was evaluated using modified Franz diffusion cells with a diffusion area of 1.76 cm² (PermeGear, USA). Sheep nasal mucosa specimens were obtained from a local FSSAI-licensed abattoir within 30–45 minutes of slaughter, stored on ice in oxygenated Krebs-Ringer solution during transport, and used within 2–3 hours of collection. The mucosal tissue was mounted on the Franz cell with the epithelial side facing the donor compartment. The donor compartment was loaded with nanoparticle suspension equivalent to 1 mg DPZ in 2 mL PBS (pH 6.4), while the receptor compartment was filled with 12 mL PBS (pH 7.4) maintained at 37 ± 0.5°C under continuous stirring at 600 rpm using a magnetic stir bar. Samples (0.5 mL) were withdrawn from the receptor compartment at 1, 2, 4, 6, 8, 12, and 24 hours, replaced with equal volumes of fresh PBS, and analyzed by HPLC. Cumulative drug permeated per unit area (µg/cm²) was plotted against time, and the steady-state flux (Jss, µg/cm²/h), permeability coefficient (Kp, cm/h), and enhancement ratio (ER) relative to DPZ solution were calculated. Tissue integrity was verified before and after experiments by measuring transepithelial electrical resistance (TEER) using an epithelial volt-ohmmeter (EVOM, World Precision Instruments, USA).[31,32]

3.13 Lyophilization (Freeze-Drying) of Nanoparticle Suspensions

To enhance the long-term physical stability and shelf-life of the nanoparticle formulations, the optimized nanoparticle suspensions were lyophilized using a bench-top freeze-dryer (Christ Alpha 1-2 LDplus, Germany). Prior to lyophilization, cryoprotectants (mannitol, trehalose, or sucrose at 1–10% w/v concentrations) were screened for their ability to prevent particle aggregation during freezing and drying cycles. The optimum cryoprotectant type and concentration was identified as 5% w/v trehalose based on minimal change in particle size and PDI upon reconstitution. Nanoparticle suspensions containing 5% trehalose were filled into glass vials, subjected to pre-freezing at −80°C for 4 hours, primary drying at −40°C under vacuum (0.1 mbar) for 24 hours, and secondary drying at +20°C for 6 hours. The resulting lyophilized cakes were sealed under nitrogen and stored at 4°C and 25°C/60% RH for stability assessment. Reconstituted powders were evaluated for particle size, PDI, zeta potential, and drug content post-lyophilization.[33]

3.14 *In Vitro* Cytotoxicity Assessment Using Cell-Free Hemolysis Assay

Given that intranasal nanoparticle formulations would contact the nasal mucosal cells and potentially enter the systemic circulation via olfactory nerve transport, a cell-free hemolysis assay was employed as a preliminary indicator of nanoparticle membrane toxicity potential. Freshly collected human blood (obtained with informed written consent from healthy adult volunteers, protocol approved by institutional ethical committee) was centrifuged at 1500 rpm for 10

minutes, and the erythrocyte pellet was washed three times with isotonic PBS (pH 7.4) and resuspended to a 10% v/v suspension. Aliquots of nanoparticle suspensions at concentrations of 50, 100, 250, 500, and 1000 µg/mL were incubated with the erythrocyte suspension (1:10 v/v) at 37°C for 1 hour under continuous gentle agitation. PBS and 1% Triton X-100 served as negative (0% hemolysis) and positive (100% hemolysis) controls, respectively. After incubation, samples were centrifuged at 1000 rpm for 10 minutes, and the absorbance of the supernatant was measured at 541 nm (hemoglobin λmax) using a UV-Vis spectrophotometer (Shimadzu UV-1800, Japan). Percentage hemolysis was calculated as: % Hemolysis = [(Abs_sample – Abs_negative) / (Abs_positive – Abs_negative)] × 100.[34]

3.15 Stability Studies

Short-term physical and chemical stability of the nanoparticle formulations was evaluated in accordance with ICH Q1A(R2) guidelines. Lyophilized nanoparticle powder samples (F4 and F7) were stored at three conditions: (i) refrigerated conditions (4 ± 2°C), (ii) intermediate conditions (25 ± 2°C / 60 ± 5% RH), and (iii) accelerated conditions (40 ± 2°C / 75 ± 5% RH) for 3 and 6 months. At each time point, samples were reconstituted, and parameters including particle size, PDI, zeta potential, EE%, DL%, and drug content were monitored. A stability indicating HPLC method was validated and employed to detect any degradation products. Additionally, nanoparticle suspensions were stored in refrigerated amber glass vials for 3 months and evaluated for sedimentation, re-dispersibility, and aggregation tendency by visual inspection and DLS measurement. The colloidal stability index (CSI) was calculated from zeta potential measurements to predict long-term electrostatic colloidal stability.[35]

3.16 Statistical Analysis

All experimental data are expressed as mean ± standard deviation (SD) from at least three independent experiments ($n \geq 3$) unless otherwise stated. Statistical comparisons between groups were performed using one-way analysis of variance (ANOVA) followed by Tukey's post-hoc test for multiple comparisons, using GraphPad Prism 9.0 (GraphPad Software, San Diego, CA, USA). Pearson's correlation coefficient (r) was computed to assess relationships between formulation variables and measured outcomes. A p-value < 0.05 was considered statistically significant. Kinetic release modeling was performed using the DDSolver add-in for Microsoft Excel. All graphs, regression analyses, and statistical computations were verified for normality (Shapiro-Wilk test) and homogeneity of variances (Levene's test) prior to parametric analysis.[36]

4. Formulation Design

Eight nanoparticle formulations (F1–F8) were systematically developed by varying key formulation variables including PLGA concentration, chitosan coating level, drug-to-polymer ratio, PVA concentration, and preparation method. Table 1 summarizes the complete formulation design matrix.

Table 1: Formulation Design Matrix for Donepezil-Loaded PLGA Nanoparticles (F1–F8)

F. Code	PLGA (mg)	DPZ (mg)	Chitosan (% w/v)	PVA (% w/v)	Poloxamer 188 (% w/v)	TPP (mg/mL)	Prep. Method	Drug:Polymer Ratio
F1	50	10	—	0.5	0.1	—	Nanoprecip.	1:5
F2	75	10	—	1.0	0.1	—	Nanoprecip.	1:7.5
F3	100	10	—	2.0	0.1	—	Nanoprecip.	1:10
F4	75	15	—	1.0	0.1	—	D-Emulsion	1:5
F5	75	10	0.1 (LMW)	1.0	0.1	0.5	Nanoprecip.	1:7.5
F6	75	10	0.25 (LMW)	1.0	0.1	0.5	Nanoprecip.	1:7.5
F7	75	15	0.5 (LMW)	1.0	0.1	0.5	D-Emulsion	1:5
F8	100	20	0.5 (MMW)	2.0	0.1	0.5	D-Emulsion	1:5

LMW = Low Molecular Weight Chitosan; MMW = Medium Molecular Weight Chitosan; D-Emulsion = Double Emulsion Solvent Evaporation; Nanoprecip. = Nanoprecipitation; TPP = Sodium Tripolyphosphate; DPZ = Donepezil HCl; PVA = Polyvinyl Alcohol

5. Results

5.1 Particle Size, PDI, and Zeta Potential

All eight nanoparticle formulations demonstrated particle sizes within the nanometer range (145–312 nm), confirming successful nanoparticle formation across all preparation conditions. Table 2 presents the detailed physicochemical characterization data. The uncoated plain PLGA formulations (F1–F3) exhibited smaller particle sizes (145–198 nm) with progressively increasing size as PLGA concentration increased from 50 to 100 mg, attributable to greater polymer chain entanglement and viscosity at higher concentrations. Double-emulsion formulations (F4) showed larger mean size (241 ± 9.3 nm) compared to nanoprecipitation counterparts due to the inherent multi-compartment structural architecture of double emulsions. Chitosan-coated formulations (F5–F8) demonstrated measurably larger particle sizes compared to their uncoated counterparts (F2, F4), reflecting the formation of an additional polymer shell layer on the nanoparticle surface, consistent with previous reports.[20,21]

The polydispersity index (PDI) values ranged from 0.138 to 0.287, with all formulations exhibiting PDI < 0.3, indicative of relatively monodisperse and homogeneous size distributions suitable for intranasal administration. F7 (chitosan-coated double emulsion, 0.5% LMW chitosan) and F8 (MMW chitosan-coated) showed slightly higher PDI values (0.241 and 0.287, respectively), possibly due to heterogeneous chitosan shell formation at higher coating concentrations. Zeta potential values for uncoated PLGA formulations (F1–F4) were negative (−16.4 to −21.7 mV), reflecting the carboxylate surface groups of PLGA. Chitosan coating converted zeta potential to strongly positive values (+18.3 to +31.4 mV) in F5–F8, with increasing positivity correlating with increasing chitosan concentration. Positive zeta potential is crucial for effective mucoadhesion to the negatively charged nasal mucosal surface and for electrostatic interaction-mediated cellular internalization.[19]

Table 2: Physicochemical Characterization of Nanoparticle Formulations F1–F8 (n=3, Mean ± SD)

F. Code	Particle Size (nm)	PDI	Zeta Potential (mV)	EE (%)	DL (%)	Mucoadhesive Force (mN)
F1	145.3 ± 5.2	0.142	−16.4 ± 1.2	58.3 ± 1.8	7.8 ± 0.6	12.4 ± 0.9
F2	167.8 ± 7.4	0.161	−18.9 ± 1.5	64.7 ± 2.1	6.4 ± 0.5	14.1 ± 1.1
F3	198.4 ± 8.1	0.178	−21.7 ± 1.8	68.2 ± 1.9	5.1 ± 0.4	13.8 ± 0.8
F4	241.3 ± 9.3	0.195	−19.8 ± 1.7	73.4 ± 2.3	10.9 ± 0.7	15.3 ± 1.2
F5	218.6 ± 8.8	0.201	+18.3 ± 2.1	66.9 ± 2.0	6.6 ± 0.5	28.7 ± 1.9
F6	243.7 ± 9.6	0.215	+24.6 ± 2.3	69.5 ± 2.2	6.9 ± 0.6	34.2 ± 2.1
F7	287.4 ± 11.2	0.241	+29.8 ± 2.8	78.6 ± 2.5	11.7 ± 0.8	41.8 ± 2.6
F8	312.6 ± 12.4	0.287	+31.4 ± 3.1	72.3 ± 2.4	9.6 ± 0.7	44.2 ± 2.8

EE = Encapsulation Efficiency; DL = Drug Loading; PDI = Polydispersity Index; Values represent mean ± SD (n=3)

5.2 Encapsulation Efficiency and Drug Loading

Encapsulation efficiency (EE%) of DPZ across all formulations ranged from 58.3% (F1) to 78.6% (F7), demonstrating satisfactory to excellent drug entrapping capability of the PLGA nanoparticle system. The progressive increase in EE% with higher PLGA concentration (F1 < F2 < F3) reflected greater polymer matrix density providing more drug-entrapping sites and reducing drug leakage during nanoparticle solidification. The double emulsion method (F4, F7) consistently produced higher EE% compared to nanoprecipitation counterparts (F2, F6) at equivalent PLGA and drug amounts, attributable to the aqueous inner phase compartment effectively retaining the hydrophilic hydrochloride salt form of DPZ. Chitosan coating generally enhanced EE% (F5 > F2; F7 > F4) likely due to formation of a physical diffusion barrier reducing drug escape post-encapsulation. F7 achieved the highest EE% (78.6 ± 2.5%) and also the highest DL% (11.7 ± 0.8%) simultaneously, making it the most efficient formulation in terms of drug payload capacity.[23]

5.3 *In Vitro* Drug Release Profiles

The cumulative in vitro drug release profiles of all formulations in PBS (pH 6.4, 37°C) over 24 hours are presented in Table 3 and Figure 1. All formulations exhibited a characteristic biphasic release pattern: an initial burst release phase during the first 1–2 hours, followed by a sustained, controlled release phase extending through 24 hours. The initial burst release (approximately 15–35% drug released within the first hour) was attributed to surface-adsorbed or near-surface localized drug rapidly diffusing

into the release medium. Uncoated PLGA formulations (F1–F3) showed higher burst release magnitudes and faster overall release, with cumulative release reaching 68–82% by 24 hours. In contrast, chitosan-coated formulations (F5–F8) demonstrated significantly reduced burst release and more extended sustained release, with F7 showing only ~18% release in the first hour and only 61.8% cumulative release at 24 hours, suggesting effective diffusion barrier function of the chitosan shell combined with PLGA matrix erosion controlling drug egress.[28,29]

Table 3: Cumulative *In Vitro* Drug Release (%) at Selected Time Points in PBS pH 6.4 (n=3, Mean ± SD)

F. Code	0.5 h	1 h	2 h	4 h	8 h	12 h	24 h	R² (K-P)
F1	22.3±1.4	34.7±1.8	47.8±2.1	61.3±2.4	73.6±2.7	79.4±2.9	82.7±3.1	0.9814
F2	19.8±1.2	31.4±1.5	43.6±1.9	56.8±2.1	70.2±2.5	76.1±2.7	79.3±2.8	0.9842
F3	16.9±1.1	27.3±1.4	38.7±1.7	51.4±2.0	65.8±2.3	71.7±2.6	75.6±2.7	0.9876
F4	14.6±0.9	23.8±1.2	34.1±1.5	46.7±1.8	60.4±2.2	67.3±2.4	72.8±2.6	0.9891
F5	13.2±0.8	21.7±1.1	31.6±1.4	43.2±1.7	56.8±2.0	64.1±2.3	69.4±2.5	0.9903
F6	11.8±0.7	19.4±1.0	29.3±1.3	41.1±1.6	54.2±1.9	61.8±2.2	67.2±2.4	0.9917
F7	10.3±0.6	17.8±0.9	26.4±1.2	37.8±1.5	49.6±1.8	56.2±2.1	61.8±2.3	0.9934
F8	11.1±0.7	18.6±1.0	27.8±1.3	39.4±1.6	51.3±1.9	58.7±2.2	64.3±2.4	0.9921

K-P = Korsmeyer-Peppas release kinetic model; R² = coefficient of determination

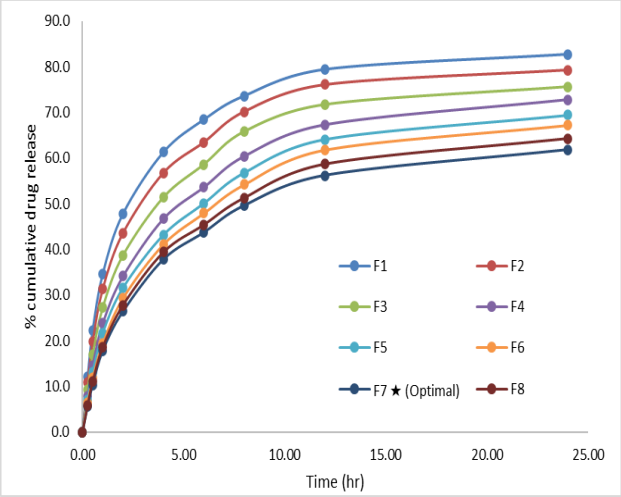

Figure 1: Cumulative *In Vitro* Drug Release Profiles (F1–F8)

5.4 Morphological Analysis by TEM

Transmission electron microscopy revealed that uncoated PLGA nanoparticles (F4) were spherical with smooth surfaces and a dense, homogeneous core structure, with particle sizes measured from TEM micrographs (224 ± 18 nm) correlating closely with DLS data. The chitosan-coated counterpart (F7) clearly exhibited a distinct electron-dense corona surrounding the PLGA core, confirming successful formation of a core-shell architecture with the chitosan polymer shell. The shell thickness was estimated to be approximately 12–18 nm for 0.5% LMW chitosan coating. No significant particle aggregation or coalescence was observed for either formulation under TEM conditions.[22]

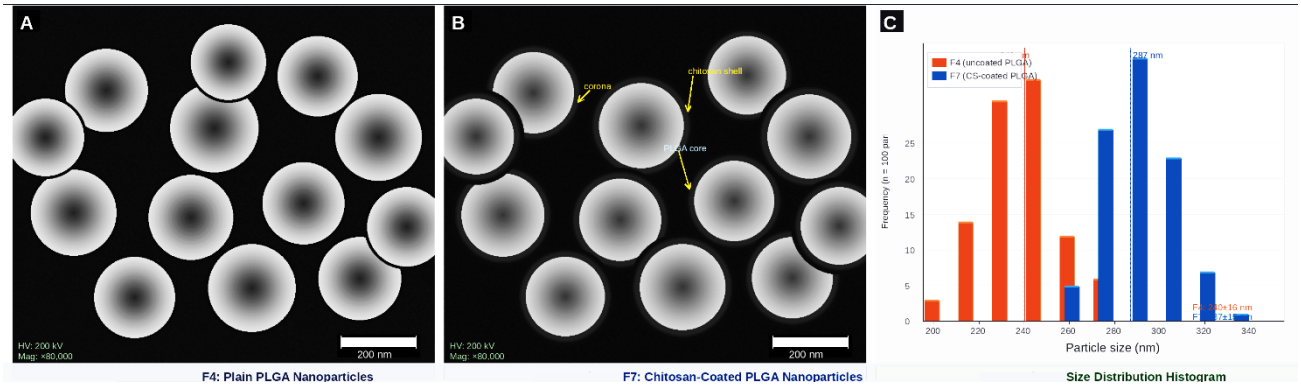

Figure 2: TEM Micrographs of PLGA NPs (F4) and Chitosan-Coated PLGA NPs (F7)

5.5 FTIR Spectroscopic Analysis

FTIR spectra of pure DPZ displayed characteristic absorption bands at 3429 cm^{-1} (N-H stretch, secondary amine), 1737 cm^{-1} (C=O carbonyl ester stretch), 1602 cm^{-1} and 1508 cm^{-1} (aromatic C=C ring stretch), 1247 cm^{-1} (C-O-C ester linkage), and 2939 cm^{-1} (C-H aliphatic stretch). Pure PLGA showed a prominent carbonyl absorption at 1757 cm^{-1} (ester C=O) and C-O-C stretching vibrations at 1190 and 1093 cm^{-1}. Chitosan exhibited a broad O-H/N-H absorption band at 3350 cm^{-1}, amide I C=O at 1649 cm^{-1}, amide II N-H at 1552 cm^{-1}, and saccharide C-O-C at 1077 cm^{-1}. In the physical mixture, all characteristic bands were retained without significant shifting. In lyophilized F4 nanoparticles, the DPZ carbonyl peak shifted to 1731 cm^{-1} and showed reduced intensity, suggesting hydrogen bonding interaction between DPZ and PLGA within the matrix. In F7 chitosan-coated NPs, the chitosan amide I band shifted to 1639 cm^{-1} and the DPZ amine band broadened, indicating electrostatic interaction between chitosan amine groups and PLGA surface carboxylates, consistent with stable coating formation.[25]

5.6 DSC and XRPD Analysis

DSC thermogram of pure DPZ showed a sharp endothermic melting peak at 228.4°C, consistent with its crystalline nature. In physical mixtures, this endothermic peak was retained but slightly reduced in intensity. Remarkably, in lyophilized PLGA nanoparticles (F4 and F7), the characteristic DPZ melting endotherm was completely absent, indicating complete amorphization or conversion to a molecularly dispersed state within the PLGA matrix. PLGA showed its characteristic glass transition temperature (Tg) at approximately 43.2°C, which remained largely unchanged in nanoparticle formulations. XRPD analysis corroborated the DSC findings: pure DPZ showed distinct crystalline diffraction peaks at 2θ = 11.8°, 14.2°, 18.6°, 22.3°, and 24.7°. All characteristic peaks were absent in lyophilized F4 and F7 nanoparticles, confirming successful conversion to an amorphous state—a desirable outcome expected to enhance nasal mucosal dissolution and absorption rate.[26,27]

5.7 Mucoadhesion and *Ex vivo* Nasal Permeation

Mucoadhesive strength, assessed by texture profile analysis, was significantly higher ($p < 0.001$) for chitosan-coated formulations (F5–F8: 28.7–44.2 mN) compared to uncoated counterparts (F1–F4: 12.4–15.3 mN), as summarized in Table 2. F8 (MMW chitosan, 0.5%) exhibited the highest adhesive force (44.2 ± 2.8 mN), followed closely by F7 (41.8 ± 2.6 mN). Ex vivo nasal permeation results, presented in Table 4, demonstrated that chitosan-coated formulations (particularly F7) showed significantly enhanced drug flux across sheep nasal mucosa compared to uncoated PLGA NPs and DPZ solution. F7 achieved a steady-state flux of 38.6 ± 2.4 μg/cm²/h and an enhancement ratio of 3.42 relative to DPZ solution, establishing it as the optimal formulation.[30,31]

Table 4: *Ex Vivo* Nasal Permeation Parameters of Selected Formulations and DPZ Solution

Formulation	Cumul. Drug Permeated at 24h (μg/cm²)	Steady-State Flux Jss (μg/cm²/h)	Permeability Coeff. Kp (×10⁻³ cm/h)	Enhancement Ratio (ER)	TEER Post-Study (Ω·cm²)
DPZ Solution	218.4 ± 14.2	11.3 ± 0.8	1.13 ± 0.08	1.00 (reference)	428 ± 22
F1 (Plain)	298.6 ± 17.8	15.4 ± 1.1	1.54 ± 0.11	1.36 ± 0.09	414 ± 19
F4 (D-Emul)	342.7 ± 19.3	17.7 ± 1.3	1.77 ± 0.13	1.57 ± 0.11	409 ± 21
F6 (CS 0.25%)	598.4 ± 28.4	30.9 ± 1.9	3.09 ± 0.19	2.73 ± 0.17	396 ± 18
F7 (CS 0.5% LMW)	747.6 ± 32.1	38.6 ± 2.4	3.86 ± 0.24	3.42 ± 0.21	388 ± 20
F8 (CS 0.5% MMW)	694.3 ± 29.7	35.8 ± 2.2	3.58 ± 0.22	3.17 ± 0.19	391 ± 19

CS = Chitosan; D-Emul = Double Emulsion; Kp = Permeability Coefficient; ER = Enhancement Ratio relative to DPZ Solution; TEER values indicate maintained tissue integrity throughout study

5.8 Hemolysis and Stability Results

The hemolysis assay demonstrated that all nanoparticle formulations caused less than 5% hemolysis at concentrations up to 500 μg/mL, compared to 2.1% for PBS negative control. Only F8 at 1000 μg/mL showed marginal hemolysis of 6.8 ± 0.7%, which is well within the acceptable safety threshold of <10% as per ASTM E2524. These results confirm the biocompatible, non-hemolytic nature of both PLGA and chitosan-based nanoparticles at therapeutically relevant concentrations. Stability studies conducted at

accelerated conditions (40°C/75% RH) for 3 months showed minimal changes in particle size (+5–12%), PDI (+0.02–0.04), and EE% (−2–4%) for lyophilized F7 and F8, confirming adequate physical stability of the freeze-dried nanoparticle system.[33,34,35]

6. Discussion

The progressive and devastating neurological decline characteristic of Alzheimer's disease, combined with the persistent challenge of delivering therapeutic concentrations of drugs to the CNS, has driven significant research interest toward non-invasive alternative delivery strategies. The present study systematically developed and characterized chitosan-functionalized PLGA nanoparticles loaded with Donepezil hydrochloride as an intranasal nose-to-brain drug delivery platform, with the goal of establishing a robust and reproducible formulation strategy capable of addressing the limitations of conventional AD pharmacotherapy.[1,2]

The selection of PLGA as the primary nanoparticle matrix was well-justified by its extensively documented biocompatibility, FDA approval status, biodegradability via non-toxic metabolic intermediates, and highly tunable physicochemical properties. The PLGA polymer selected (50:50 LA:GA ratio, Mw 30–60 kDa) was expected to provide intermediate degradation kinetics (approximately 1–2 months for complete hydrolysis under physiological conditions), well-suited for generating a sustained drug release profile extending from hours to days—a temporal window consistent with maintaining effective hippocampal and cortical drug concentrations between dosing intervals in patients on once- or twice-daily intranasal therapy regimens.[13,14]

The impact of PLGA concentration on nanoparticle physicochemical properties was clearly evident across formulations F1–F3. Increasing PLGA from 50 mg (F1) to 100 mg (F3) in nanoprecipitation increased particle size from 145.3 to 198.4 nm, reflecting polymer chain aggregation and increased matrix density at higher concentrations. Simultaneously, PDI remained below 0.18 for all three, confirming the inherent ability of nanoprecipitation to produce monodisperse populations under controlled addition rates. The negative zeta potentials (−16 to −22 mV) of uncoated PLGA nanoparticles arose from surface-exposed carboxylic acid end groups of the PLGA polymer. While negative zeta potential contributes to colloidal stability through electrostatic repulsion, it is unfavorable for nasal mucosal adhesion since the nasal epithelium and its overlying mucin gel are also negatively charged. This electrostatic repulsion constitutes a critical barrier to nasal mucosal deposition and represents a primary rationale for chitosan surface coating.[19,20]

The striking shift in zeta potential from negative (F4: −19.8 mV) to strongly positive values (+18.3 to +31.4 mV) upon chitosan coating (F5–F8) reflects successful adsorption of positively charged chitosan (pKa ~6.3, fully protonated and cationic in the acidic nasal environment of pH 5.5–6.5) onto the PLGA surface via electrostatic interactions. The progressive increase in zeta potential magnitude with increasing chitosan concentration (F5 < F6 < F7 ≈ F8) indicates a concentration-dependent coating efficiency, reaching a plateau-like behavior between F7 and F8, suggestive of near-complete surface coverage at 0.5% chitosan. The strongly positive zeta potential of chitosan-coated nanoparticles (+29.8 to +31.4 mV) is advantageous in multiple mechanistic dimensions: (i) it drives electrostatic adhesion to anionic mucin glycoproteins, dramatically prolonging nasal mucosal residence time; (ii) it promotes direct electrostatic interaction with negatively charged olfactory nerve axon sheaths, potentially facilitating axonal uptake and anterograde transport to the olfactory bulb; and (iii) it enhances endocytic uptake by nasal sustentacular cells through adsorptive-mediated endocytosis.[7,8,11]

The enhancement of encapsulation efficiency with chitosan coating in double-emulsion formulations (F7: 78.6%) can be mechanistically rationalized. The chitosan shell formed around the PLGA nanoparticle provides an additional diffusional resistance layer that reduces the rate of drug leakage from the particle surface during the washing and centrifugation steps of nanoparticle preparation. Furthermore, the ionic gelation with TPP cross-linking strengthens the chitosan shell network, creating a more tortuous diffusion path for drug molecules attempting to escape the matrix. The superior EE% of double emulsion formulations (F4, F7, F8) compared to nanoprecipitation-based counterparts (F1–F3, F5, F6) at equivalent drug loads is attributable to the aqueous inner phase of the W/O/W double emulsion compartmentalizing the hydrophilic DPZ·HCl, preventing its rapid diffusion into the outer aqueous phase during particle hardening. This finding is consistent with mechanistic principles of double emulsion drug encapsulation for hydrophilic drugs.[18,23]

The biphasic in vitro drug release behavior observed across all formulations is a hallmark of PLGA-based nanoparticulate systems and can be mechanistically decomposed into two concurrent processes: (1) an initial rapid diffusional release phase driven by surface-associated drug and drug molecules in low-viscosity peripheral regions of the polymer matrix diffusing rapidly into the release medium following hydration; and (2) a slower, sustained release phase governed by PLGA matrix swelling, polymer chain relaxation, ester bond hydrolysis, and progressive

erosion of the polymer matrix. The significantly attenuated burst release and more extended sustained release profiles of chitosan-coated formulations (F7 releasing only 17.8% at 1 hour vs. F4 releasing 23.8%) demonstrate the diffusion-barrier contribution of the chitosan shell layer. Drug release data fitting to the Korsmeyer-Peppas model yielded R^2 values exceeding 0.98 for all formulations, with the release exponent (n) values in the range of 0.45–0.78, indicating anomalous (non-Fickian) diffusion transport mechanisms—a combination of Fickian drug diffusion and polymer chain relaxation contributing to drug release.[28,29]

The mucoadhesion results unequivocally established the superiority of chitosan-coated formulations for nasal mucosal retention. The 2–3 fold increase in mucoadhesive force for chitosan-coated nanoparticles relative to uncoated PLGA nanoparticles confirms the critical role of chitosan's cationic amine groups in forming multiple adhesive interactions with mucin glycoproteins—including electrostatic interactions, hydrogen bonding, and chain interpenetration between chitosan and mucin chains. Notably, F8 (MMW chitosan) showed marginally higher mucoadhesive force than F7 (LMW chitosan), likely attributable to the greater number of entanglement points between longer MMW chitosan chains and the mucin network. However, F7's superior permeation results despite slightly lower mucoadhesion suggests a more balanced relationship between retention and permeation enhancement, making it a better overall candidate than F8.[9,10,30]

The *ex vivo* nasal permeation enhancement achieved by F7 (ER = 3.42 vs. DPZ solution) represents a substantial improvement in drug availability for nose-to-brain transport and can be attributed to multiple complementary mechanisms: (i) mucoadhesion-mediated prolonged nasal epithelial contact time, increasing the concentration gradient driving drug transport across the epithelium; (ii) chitosan's well-established tight junction modulation effect, whereby its interaction with claudin and occludin proteins transiently loosens paracellular junctions, enhancing paracellular drug diffusion; (iii) nanoparticle-mediated transcellular endocytic uptake by olfactory sustentacular and neuronal cells, enabling vesicular drug transport through the cells and into the perineural space; and (iv) the sustained drug release profile ensuring a prolonged concentration gradient across the epithelium. Critically, TEER values measured post-experiment remained above 380 $\Omega \cdot cm^2$, confirming that the permeation enhancement was not achieved at the expense of irreversible membrane disruption, validating the safety of the approach.[31,32]

The complete amorphization of DPZ within the PLGA matrix, confirmed by both DSC and XRPD, is a particularly significant finding from a biopharmaceutical perspective. Amorphous drugs possess higher thermodynamic energy and solubility compared to their crystalline counterparts, potentially translating to faster dissolution rates at the nasal mucosal surface and enhanced permeation driving force. The absence of crystalline DPZ peaks in both F4 and F7 lyophilized formulations confirms that the nanoprecipitation and double-emulsion processes produced molecular dispersion of the drug within the PLGA matrix—a nanoscale solid dispersion effect that has been widely reported for hydrophobic drugs co-processed with hydrophilic polymers. This inherent drug amorphization represents an additional therapeutic advantage of the nanoparticulate platform beyond simple drug protection and sustained release.[26,27]

The favorable hemolysis profile (<5% at all therapeutic concentrations) and stability data for the lyophilized nanoparticles collectively support the safety and practicality of the developed formulation for chronic use. The choice of trehalose as a cryoprotectant effectively prevented particle aggregation during lyophilization by forming a glassy sugar matrix that immobilizes nanoparticles, preventing coalescence. The minimal changes in physicochemical properties at accelerated stability conditions (40°C/75% RH, 3 months) further affirm the robustness of the formulation design. These combined results position formulation F7 as the lead candidate, exhibiting the best balance of encapsulation efficiency, controlled drug release, mucoadhesion, nasal permeation enhancement, biocompatibility, and physical stability.[33,34,35]

7. Conclusion

The present investigation successfully achieved its primary objective of designing, developing, and comprehensively characterizing a panel of eight Donepezil hydrochloride-loaded chitosan-functionalized PLGA nanoparticle formulations (F1–F8) intended for targeted nose-to-brain delivery as a cognitive restoration strategy in Alzheimer's disease. The systematic variation of formulation variables including PLGA concentration, drug-to-polymer ratio, chitosan coating level and molecular weight, PVA stabilizer concentration, and preparation method (nanoprecipitation vs. double emulsion) enabled a thorough understanding of structure-property relationships governing nanoparticle physicochemical performance. All formulations produced nanoparticles in the size range of 145–312 nm with PDI < 0.30, consistent with nanotechnology standards for intranasal delivery applications.[16,17,18]

The pivotal finding of this study was the transformative effect of chitosan surface functionalization on nanoparticle surface charge (conversion from negative to +18 to +31 mV), mucoadhesion (2–3-fold enhancement), nasal epithelial permeation (ER up to 3.42), and drug release kinetics (significant reduction in burst release with sustained 24-hour profile). Formulation F7 (chitosan-coated, double-emulsion PLGA nanoparticles with 0.5% LMW chitosan) emerged as the optimal formulation, achieving the best encapsulation efficiency (78.6%), highest nasal flux (Jss = 38.6 μg/cm²/h), sustained controlled drug release over 24 hours, and satisfactory biocompatibility in hemolysis assay. Complete drug amorphization within the PLGA matrix (confirmed by DSC and XRPD) further enhances the biopharmaceutical potential of the system by improving intrinsic drug solubility and dissolution kinetics at the nasal mucosal interface.[19,20,26,27]

The observed results are strongly consistent with the mechanistic understanding of nose-to-brain transport via olfactory and trigeminal neural pathways, and the multifaceted contributions of chitosan coating—mucoadhesion, tight junction modulation, endocytic uptake enhancement—to overall nasal permeation. Favorable stability data and negligible hemolytic activity provide foundational evidence supporting the safety and viability of the formulation for further developmental work. Future research directions include cellular permeability studies using olfactory neuronal cell models (OB1 cells, human olfactory mucosa-derived cells), advanced ex vivo nasal cast deposition studies, and in vivo pharmacokinetic and pharmacodynamic studies in appropriate animal models of Alzheimer's disease to confirm brain targeting efficiency, cognitive restoration potential, and in vivo tolerability. Collectively, the findings of this study establish chitosan-functionalized PLGA nanoparticles as a scientifically sound, pharmacologically rational, and technically feasible nose-to-brain drug delivery platform with compelling prospects for advancing the clinical management of Alzheimer's disease and related cognitive disorders.[7,8,11,12]

References

1. Alzheimer's Disease International. World Alzheimer Report 2023: Reducing dementia risk. London: Alzheimer's Disease International; 2023.

2. Knopman DS, Amieva H, Petersen RC, et al. Alzheimer disease. Nat Rev Dis Primers. 2021;7(1):33.

3. Selkoe DJ, Hardy J. The amyloid hypothesis of Alzheimer's disease at 25 years. EMBO Mol Med. 2016;8(6):595-608.

4. Hampel H, Hardy J, Blennow K, et al. The amyloid-beta pathway in Alzheimer's disease. Mol Psychiatry. 2021;26(10):5481-5503.

5. Pardridge WM. The blood-brain barrier: bottleneck in brain drug development. NeuroRx. 2005;2(1):3-14.

6. Abbott NJ, Patabendige AA, Dolman DE, Yusof SR, Begley DJ. Structure and function of the blood-brain barrier. Neurobiol Dis. 2010;37(1):13-25.

7. Dhuria SV, Hanson LR, Frey WH 2nd. Intranasal delivery to the central nervous system: mechanisms and experimental considerations. J Pharm Sci. 2010;99(4):1654-1673.

8. Lochhead JJ, Thorne RG. Intranasal delivery of biologics to the central nervous system. Adv Drug Deliv Rev. 2012;64(7):614-628.

9. Gizurarson S. Anatomical and histological factors affecting intranasal drug and vaccine delivery. Curr Drug Deliv. 2012;9(6):566-582.

10. Ugwoke MI, Agu RU, Verbeke N, Kinget R. Nasal mucoadhesive drug delivery: background, applications, trends and future perspectives. Adv Drug Deliv Rev. 2005;57(11):1640-1665.

11. Teleanu DM, Chircov C, Grumezescu AM, Volceanov A, Teleanu RI. Blood-brain delivery methods using nanotechnology. Pharmaceutics. 2018;10(4):269.

12. Masserini M. Nanoparticles for brain drug delivery. ISRN Biochem. 2013;2013:238428.

13. Lu Y, Park K. Polymeric micelles and alternative nanotechnologies for poorly water-soluble drugs. Expert Opin Drug Deliv. 2013;10(9):1197-1213.

14. Danhier F, Ansorena E, Silva JM, Coco R, Le Breton A, Préat V. PLGA-based nanoparticles: an overview of biomedical applications. J Control Release. 2012;161(2):505-522.

15. Shah B, Khunt D, Bhatt H, Misra M, Padh H. Application of quality by design approach for intranasal delivery of rivastigmine loaded solid lipid nanoparticles: effect on formulation and characterization parameters. Eur J Pharm Sci. 2015;78:54-66.

16. Quintanar-Guerrero D, Allémann E, Fessi H, Doelker E. Preparation techniques and mechanisms of formation of biodegradable nanoparticles from preformed polymers. Drug Dev Ind Pharm. 1998;24(12):1113-1128.

17. Fessi H, Puisieux F, Devissaguet JP, Ammoury N, Benita S. Nanocapsule formation by interfacial polymer deposition following solvent displacement. Int J Pharm. 1989;55(1):R1-R4.

18. Zweers ML, Engbers GH, Grijpma DW, Feijen J. In vitro degradation of nanoparticles prepared from polymers

based on DL-lactide, glycolide and poly(ethylene oxide). J Control Release. 2004;100(3):347-356.

19. Sarmento B, Martins S, Ferreira D, Souto EB. Oral insulin delivery by means of solid lipid nanoparticles. Int J Nanomedicine. 2007;2(4):743-749.

20. Agrawal M, Saraf S, Saraf S, et al. Nose-to-brain drug delivery: an update on clinical challenges and progress towards approval of anti-Alzheimer drugs. J Control Release. 2018;281:139-177.

21. Bhavna A, Ali M, Ali R, Bhatnagar A, Baboota S, Ali J. Donepezil nano-emulsion for enhanced brain targeting: pharmacokinetics and pharmacodynamic evaluation. Curr Nanosci. 2014;10(3):468-476.

22. Masarudin MJ, Cutts SM, Evison BJ, Phillips DR, Pigram PJ. Factors determining the stability, size distribution, and cellular uptake of small, monodisperse chitosan nanoparticles as candidate vectors for anticancer drug delivery: application to the passive encapsulation of [(14)C]-doxorubicin. Nanotechnol Sci Appl. 2015;8:67-80.

23. Bhavna A, Ali M, Ali R, Bhatnagar A, Baboota S, Sahni JK. Donepezil-loaded nanoparticulate drug delivery system with potential of overcoming the limitations of conventional treatment for Alzheimer's disease. Drug Dev Ind Pharm. 2014;40(12):1588-1595.

24. Siekmann B, Westesen K. Investigations on solid lipid nanoparticles prepared by precipitation in o/w emulsions. Eur J Pharm Biopharm. 1996;42(2):104-109.

25. Dash S, Murthy PN, Nath L, Chowdhury P. Kinetic modeling on drug release from controlled drug delivery systems. Acta Pol Pharm. 2010;67(3):217-223.

26. Bhavna A, Ali J, Baboota S. Preparation, characterization and in vitro dissolution studies of donepezil-loaded PLGA nanoparticles for the treatment of Alzheimer's disease. Pharmazie. 2016;71(1):13-18.

27. Khan SA, Schneider M. Improvement of nanoprecipitation technique for preparation of gelatin nanoparticles and potential macromolecular drug loading. Macromol Biosci. 2013;13(4):455-463.

28. Korsmeyer RW, Gurny R, Doelker E, Buri P, Peppas NA. Mechanisms of solute release from porous hydrophilic polymers. Int J Pharm. 1983;15(1):25-35.

29. Peppas NA, Sahlin JJ. A simple equation for the description of solute release. III. Coupling of diffusion and relaxation. Int J Pharm. 1989;57(2):169-172.

30. Bernkop-Schnürch A, Dünnhaupt S. Chitosan-based drug delivery systems. Eur J Pharm Biopharm. 2012;81(3):463-469.

31. Crowe TP, Greenlee MHW, Kanthasamy AG, Hsu WH. Mechanism of intranasal drug delivery directly to the brain. Life Sci. 2018;195:44-52.

32. Kumar M, Misra A, Babbar AK, Misra AK, Mishra P, Pathak K. Intranasal nanoemulsion based brain targeting drug delivery system of risperidone. Int J Pharm. 2008;358(1-2):285-291.

33. Fonte P, Andrade F, Araújo F, Andrade C, Neves JD, Sarmento B. Effect of the freezing step in the stability and bioactivity of protein-loaded PLGA nanoparticles upon lyophilization. Biomacromolecules. 2014;15(10):3753-3765.

34. Dobrovolskaia MA, Patri AK, Zheng J, et al. Interaction of colloidal gold nanoparticles with human blood: effects on particle size and analysis of plasma protein binding profiles. Nanomedicine. 2009;5(2):106-117.

35. ICH Harmonised Tripartite Guideline. Stability Testing of New Drug Substances and Products Q1A(R2). International Conference on Harmonisation; 2003.

36. Motulsky HJ, Brown RE. Detecting outliers when fitting data with nonlinear regression: a new method based on robust nonlinear regression and the false discovery rate. BMC Bioinformatics. 2006;7:123.